

On the Use of QuikSCAT Scatterometer Measurements of Surface Winds for Marine Weather Prediction

DUDLEY B. CHELTON AND MICHAEL H. FREILICH

College of Oceanic and Atmospheric Sciences, and Cooperative Institute for Oceanographic Satellite Studies, Oregon State University, Corvallis, Oregon

JOSEPH M. SIENKIEWICZ AND JOAN M. VON AHN

Ocean Prediction Center, National Oceanic and Atmospheric Administration/National Centers for Environmental Prediction, Camp Springs, Maryland

(Manuscript received 9 September 2005, in final form 22 December 2005)

ABSTRACT

The value of Quick Scatterometer (QuikSCAT) measurements of 10-m ocean vector winds for marine weather prediction is investigated from two Northern Hemisphere case studies. The first of these focuses on an intense cyclone with hurricane-force winds that occurred over the extratropical western North Pacific on 10 January 2005. The second is a 17 February 2005 example that is typical of sea surface temperature influence on low-level winds in moderate wind conditions in the vicinity of the Gulf Stream in the western North Atlantic. In both cases, the analyses of 10-m winds from the NCEP and ECMWF global numerical weather prediction models considerably underestimated the spatial variability of the wind field on scales smaller than 1000 km compared with the structure determined from QuikSCAT observations. The NCEP and ECMWF models both assimilate QuikSCAT observations. While the accuracies of the 10-m wind analyses from these models measurably improved after implementation of the QuikSCAT data assimilation, the information content in the QuikSCAT data is underutilized by the numerical models. QuikSCAT data are available in near-real time in the NOAA/NCEP Advanced Weather Interactive Processing System (N-AWIPS) and are used extensively in manual analyses of surface winds. The high resolution of the QuikSCAT data is routinely utilized by forecasters at the NOAA/NCEP Ocean Prediction Center, Tropical Prediction Center, and other NOAA weather forecast offices to improve the accuracies of wind warnings in marine forecasts.

1. Introduction

Satellite scatterometer measurements of 10-m vector winds were recently used to assess the accuracies of surface wind fields in the National Centers for Environmental Prediction (NCEP) and European Centre for Medium-Range Weather Forecasts (ECMWF) global numerical weather prediction (NWP) models (Chelton and Freilich 2005, hereafter CF05). The period February 2002–January 2003 is of particular interest, as this corresponded to the first 12 months of assimilation of SeaWinds scatterometer data from the Quick Scatterometer (QuikSCAT) satellite into both of

these NWP models. The statistical comparisons clearly showed the positive impact of this assimilation in both models. As pointed out by Leslie and Buckley (2006), however, the bulk statistics presented by CF05 understate the value of scatterometer data for improving the forecast accuracy of extreme weather events in data-sparse regions of the World Ocean. Their two manual analyses demonstrating the utility of scatterometry in the Southern Hemisphere where in situ observations are particularly sparse add to the ever-growing number of case studies of the positive impact of scatterometry on marine weather prediction and on understanding the development of extreme weather events over the open ocean (e.g., Atlas et al. 2001, 2005a,b; Sharp et al. 2002; Yeh et al. 2002; Leidner et al. 2003; and others). In this study, we present two new case studies that show that the impact of scatterometry is not limited to Southern Hemisphere data-sparse regions or to extreme events,

Corresponding author address: Dudley B. Chelton, College of Oceanic and Atmospheric Sciences, 104 COAS Administration Building, Oregon State University, Corvallis, OR 97331-5503.
E-mail: chelton@coas.oregonstate.edu

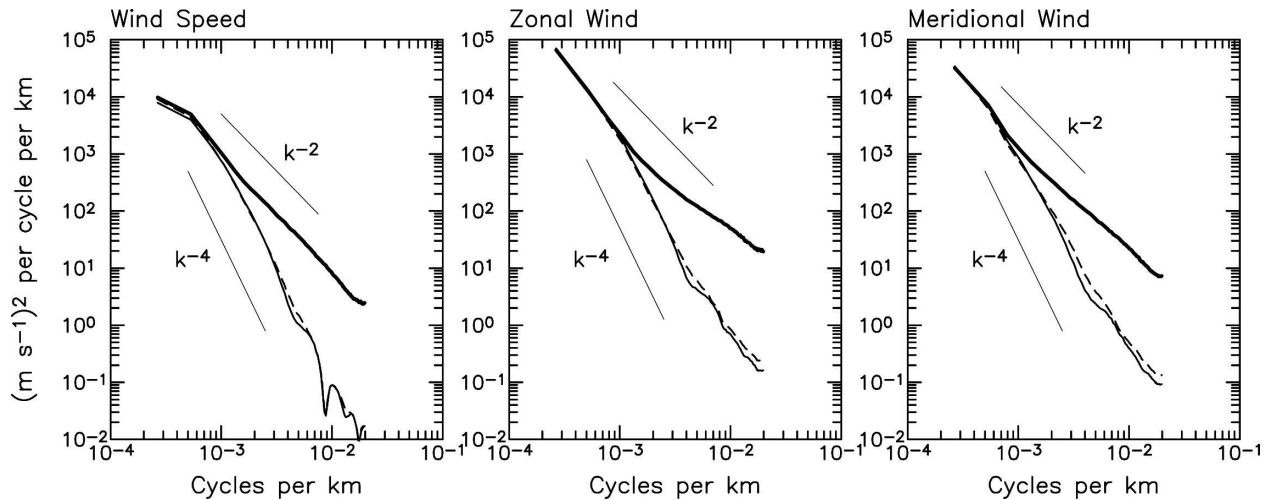


FIG. 1. Along-track wavenumber spectra of (a) wind speed and the (b) zonal and (c) meridional wind components in the eastern North Pacific computed from QuikSCAT observations (heavy solid lines), NCEP analyses (thin solid lines), and ECMWF analyses (dashed lines) of 10-m winds bilinearly interpolated to the times and locations of the QuikSCAT observations. Lines corresponding to spectral dependencies of k^{-2} and k^{-4} on along-track wavenumber k are shown on each panel for reference. The spectra were computed from the middle 1600 km of each ascending and descending QuikSCAT measurement swath, excluding the near-nadir measurements within ± 125 km of the QuikSCAT ground track (see Chelton and Freilich 2005) within the geographical region bounded by 20° – 50° N and 155° – 120° W. The QuikSCAT winds were smoothed a small amount on a swath-by-swath basis using a loess smoother (Schlax et al. 2001) with a half-power filter cutoff at a wavelength of about 60 km. The individual spectra for each incidence angle that included at least 150 consecutive along-track observations were ensemble averaged over the off-nadir incidence angles and over calendar year 2004. The structure at the highest wavenumbers in the wind speed spectra from NCEP and ECMWF is an artifact of the bilinear interpolation of the gridded wind fields to the QuikSCAT observation locations.

and that the information content of scatterometer data is considerably underutilized in the assimilation procedures of the NCEP and ECMWF models. We also discuss the validity of QuikSCAT wind retrievals in raining conditions.

2. Resolution

The technique of radar scatterometry is summarized in detail by CF05. Briefly, wind speed and direction are obtained by combining measurements of radar backscatter from a given location on the sea surface at multiple antenna look angles. For QuikSCAT, these multiple viewing angles are facilitated by the movement of the satellite along its orbit that provides forward and aft views from four different measurement geometries within a time interval of 4.5 min. The accuracy of the wind retrievals is best characterized in terms of vector component errors (Freilich and Dunbar 1999); the QuikSCAT accuracy is about 0.75 m s^{-1} in the along-wind component and about 1.5 m s^{-1} in the crosswind component (CF05). Wind direction accuracy is thus a sensitive function of wind speed at low wind speeds but improves rapidly with increasing wind speed. At wind speeds higher than about 6 m s^{-1} , the QuikSCAT directional accuracy is about 14° . In general, the

accuracies of QuikSCAT wind retrievals are degraded when rain significantly contaminates the radar footprint. When the wind speed is sufficiently strong, however, accurate winds can often be retrieved even in raining conditions (Milliff et al. 2004; see also section 4).

Scatterometry provides far more extensive geographical and temporal coverage and higher spatial resolution of ocean vector winds than are obtained by any other means. In the standard processing of the QuikSCAT data, the radar backscatter measurements are binned in 25-km areas for vector wind retrievals (see Fig. 4 of CF05). The high resolution of scatterometer wind observations can be quantified from along-track wavenumber spectral analysis (e.g., Freilich and Chelton 1986; Wikle et al. 1999; Milliff et al. 1999, 2004; Patoux and Brown 2001). The heavy solid lines in Fig. 1 are the wavenumber spectra of the QuikSCAT zonal and meridional wind components and the wind speed in the eastern North Pacific. In all three variables, the dependence on wavenumber k drops off as approximately k^{-2} at low wavenumbers. The wavenumber roll-off is somewhat flatter at wavelengths shorter than about 1000 km (i.e., wavenumbers higher than about 10^{-3} cycles per kilometer).

For comparison, the wavenumber spectra computed

from the 10-m analyzed wind fields from the operational global NCEP and ECMWF models are shown in Fig. 1 as the thin solid and dashed lines, respectively. At wavelengths longer than about 1000 km, the NCEP and ECMWF spectra are almost indistinguishable from the QuikSCAT spectra. At shorter wavelengths (higher wavenumbers), however, the NCEP and ECMWF spectra drop off steeply as approximately k^{-4} . Both of these NWP models are global spectral models with triangular truncation Gaussian latitude–longitude grids. Throughout the calendar year 2004 over which the spectra in Fig. 1 were computed, the spherical harmonic resolution of the NCEP model was T254 with a quadratically conserving grid, which corresponds to an equivalent grid resolution of about 53 km (S. Lord and J. Sela 2005, personal communication). The spherical harmonic resolution of the ECMWF model was T511 with a linearly conserving grid, which corresponds to an equivalent grid resolution of about 39 km (H. Hersbach 2005, personal communication). Despite these high grid resolutions, it is evident from Fig. 1 that both models considerably underestimate the variance on scales smaller than about 1000 km. At a wavelength of 100 km, for example, the variance is underestimated by about two orders of magnitude compared with QuikSCAT. The NCEP and ECMWF models thus generally underestimate the intensity of all synoptic-scale wind variability over the open ocean, not just extreme events and not just in data-sparse regions.

High-resolution scatterometer data clearly have the potential to improve the accuracy and resolution of the low-level wind fields in NWP models. This was demonstrated from case studies of tropical cyclones by Leidner et al. (2003), who showed that assimilating the 50-km resolution winds from the National Aeronautics and Space Administration (NASA) Scatterometer (NSCAT; the predecessor to QuikSCAT) improved the ECMWF forecasts. NCEP and ECMWF began assimilating QuikSCAT winds operationally on 13 and 22 January 2002, respectively. The resulting improvements in the accuracies of these NWP models during the first year of QuikSCAT data assimilation are evident from the statistics presented by CF05. These accuracy improvements occurred abruptly after implementation of the QuikSCAT assimilation procedure in each model. This is evident, for example, from the time series of the global percentage of wind direction differences less than 20° between QuikSCAT and the two NWP models shown in Fig. 2. Significant improvements in this measure of agreement between the different wind estimates occurred immediately after 13 January 2002 in the NCEP model and immediately after 22 January 2002 in the ECMWF model.

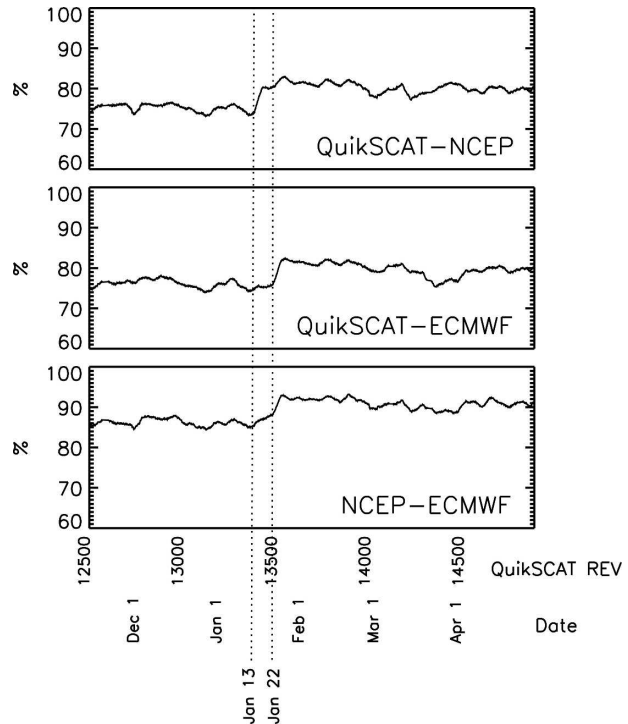


FIG. 2. Daily time series of the percentages of collocated winds with directional differences less than 20° between 15 Nov 2001 and 1 Mar 2002. The NCEP and ECMWF models began assimilating QuikSCAT winds on 13 Jan 2002 and 22 Jan 2002, respectively. Comparisons of (top) QuikSCAT vs NCEP winds, (middle) QuikSCAT vs ECMWF winds, and (bottom) NCEP vs ECMWF winds. As in Fig. 1, the statistics were computed over the middle 1600 km of the QuikSCAT measurement swath, excluding the near-nadir measurements within ± 125 km of the QuikSCAT ground track. Each time series was smoothed with a 4-day running average.

The spectra in Fig. 1 were computed by collocating the NCEP and ECMWF wind fields to the QuikSCAT observation times and locations and then ensemble averaging the individual spectra from each of the QuikSCAT overpasses during calendar year 2004. This was the third year of QuikSCAT data assimilation in the NCEP and ECMWF models. While assimilation of QuikSCAT winds measurably improved the accuracies of both of these operational models (CF05), the spatial resolution differences in Fig. 1 persist.

It is noteworthy that the QuikSCAT data are assimilated into the models in smoothed form by averaging the 25-km measurements of radar backscatter into “superobs” with resolutions of 50 km for the ECMWF model (H. Hersbach 2005, personal communication) and 0.5° for the NCEP model (1° prior to 11 March 2003) (S. Lord 2005, personal communication). Smoothing the scatterometer measurements as superobs improves the accuracy of the top-ranked wind direction ambiguity for the lower-resolution retrievals

and reduces the higher noise that is present in the 25-km resolution retrievals near nadir (Portabella and Stoffelen 2004; see also Fig. 6 of CF05). However, this smoothing cannot account for the underestimates of small-scale variability in the models since the model wind fields are deficient on much longer scales, approaching 1000 km (Fig. 1).

A more likely explanation for the underutilization of QuikSCAT information content by the models is that the global forecast and analysis systems assign overly pessimistic error estimates to the QuikSCAT wind observations. Large error estimates may ameliorate model errors that can be introduced because of inconsistencies between the coarse-resolution operational assimilation systems and the relatively high native-resolution scatterometer measurements (Isaksen and Janssen 2004). Down-weighting the QuikSCAT observations by assigning pessimistic error estimates may also be necessary to avoid disruption of the models because they are so highly optimized to other sources of input data (Leidner et al. 2003).

3. Northern Hemisphere case studies

The value of the high-resolution QuikSCAT data for marine weather prediction and the underutilization of the information content of the QuikSCAT data in the NCEP and ECMWF numerical models is demonstrated in this section from two case studies, both of which are in the Northern Hemisphere where in situ data are much more plentiful, though often still sparse, than in the Southern Hemisphere examples considered by Leslie and Buckley (2006). The new case studies considered here are recent examples of the use of QuikSCAT winds in operational weather prediction at the National Oceanic and Atmospheric Administration (NOAA) Ocean Prediction Center (OPC), which has responsibility for marine forecasts and wind warnings within the latitude range 30° – 67° N between 160° E in the North Pacific and 35° W in the North Atlantic. This area encompasses the heavily traveled trade routes between the United States and the North Pacific Rim nations, and between the United States and Europe. OPC wind warnings are routinely used by mariners to avoid severe weather conditions.

a. Case 1: The western North Pacific

The first case study considered here is an extratropical cyclone that occurred over the western North Pacific on 10 January 2005. QuikSCAT winds from an overpass at 0752 UTC (upper panel of Fig. 3) revealed a relatively small but intense cyclone centered at about 42° N, 164° E, with hurricane-force winds (i.e., greater

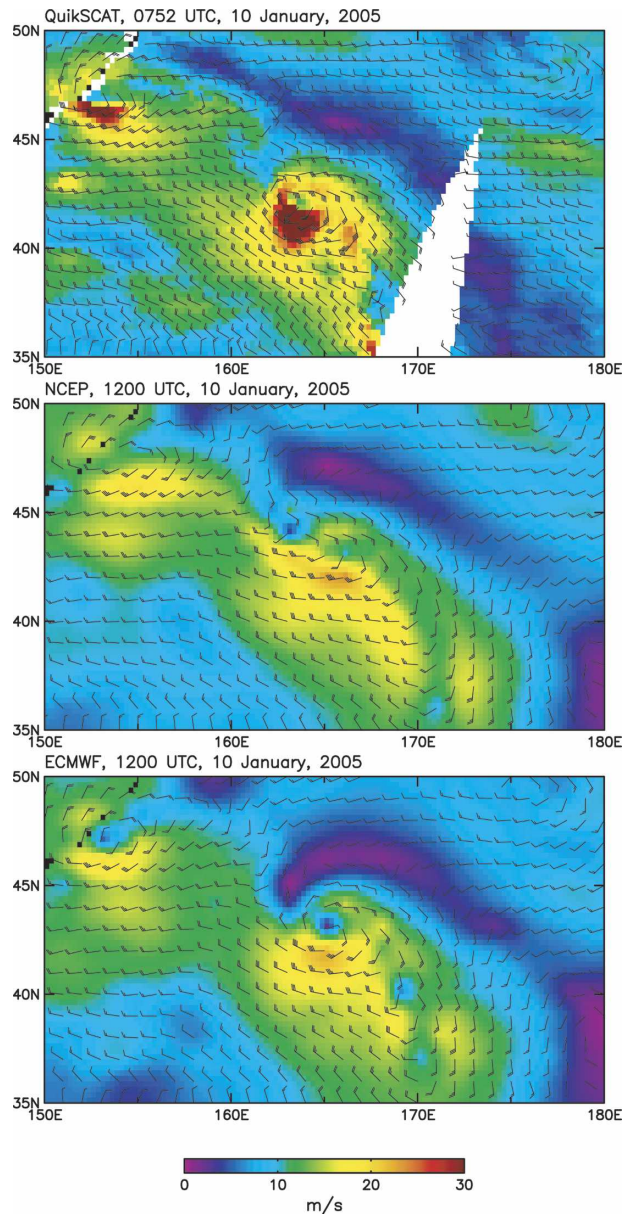


FIG. 3. The wind fields in the western North Pacific on 10 Jan 2005 constructed for the times indicated on each panel from (top) QuikSCAT observations of 10-m winds, and from analyses of 10-m winds by the (middle) NCEP and (bottom) ECMWF global numerical weather prediction models. Following meteorological convention, the wind barbs are in knots. The color scale corresponds to the wind speed in m s^{-1} . The QuikSCAT data were bin averaged in 0.25° lat \times 0.25° lon areas. For clarity, the QuikSCAT wind vectors are plotted on a $0.75^{\circ} \times 0.75^{\circ}$ grid. The NCEP and ECMWF wind vectors are plotted on a $1^{\circ} \times 1^{\circ}$ grid.

than 32.7 m s^{-1}) to the south and southwest of the cyclone center. Two of the assimilated near-real-time QuikSCAT measurements had wind speeds of 41.0 m s^{-1} . Both were flagged as rain contaminated, but the winds appeared to be valid. There was also an un-

flagged QuikSCAT observation of 38.5 m s^{-1} . Flagged but valid QuikSCAT winds are commonly found in rainy conditions when the winds are strong (see, e.g., the first case study presented by Leslie and Buckley 2006). However, distinguishing legitimate values from erroneous rain-contaminated values requires careful manual assessment by a forecaster (see further discussion in section 4). In this North Pacific example, the two flagged QuikSCAT observations were interpreted by the OPC forecaster as valid wind estimates.

The 3-h forecast from the 0600 UTC 10 January 2005 run of the NCEP global forecast model (not shown here) showed a cyclone of 998-hPa central pressure mislocated nearly 230 km to the north-northwest of the cyclone center in the QuikSCAT data. The maximum wind in the NCEP forecast was 23 m s^{-1} , which is 18 m s^{-1} less than the highest winds measured by QuikSCAT. The NCEP forecast was therefore only for gale-force conditions (i.e., wind speeds in the $17.2\text{--}24.4 \text{ m s}^{-1}$ range), whereas the actual winds were hurricane force (two categories higher than gale force).

Compared with the QuikSCAT observations approximately 4 h earlier, the 1200 UTC analysis of 10-m winds from the NCEP global forecast model (middle panel of Fig. 3) considerably underestimated the intensity of the cyclone, overestimated its spatial scale, and misrepresented its spatial structure, even after assimilation of the QuikSCAT observations from the 0752 UTC overpass shown in the top panel. The maximum wind speed in the 1200 UTC NCEP analysis was only 18 m s^{-1} , which is 23 m s^{-1} less than the observed maximum in the QuikSCAT data.

The NCEP analysis also underestimated the intensity of the smaller cyclone centered at about 47°N , 152°E near the Kuril Islands in which QuikSCAT measured a maximum wind speed of 32.0 m s^{-1} (0.7 m s^{-1} below hurricane force), whereas the maximum wind in the NCEP analysis was only 19.5 m s^{-1} (gale force). The generally smoother character of the NCEP wind field is evident over the entire domain shown in Fig. 3.

The 1200 UTC analysis of 10-m winds from the ECMWF global forecast model is shown in the lower panel of Fig. 3. While the spatial structure of the ECMWF wind field is in better agreement than NCEP with the QuikSCAT observations approximately 4 h earlier, the ECMWF analysis considerably underestimated the intensity of both cyclones, despite assimilation of the QuikSCAT observations from the 0752 UTC overpass. For the southern cyclone, the maximum ECMWF wind speed was 19.5 m s^{-1} , compared with the QuikSCAT maximum of 41 m s^{-1} . For the northern cyclone, the maximum ECMWF wind speed estimate was the same as

in the NCEP analysis (19.5 m s^{-1} , which is 12.5 m s^{-1} less than the QuikSCAT maximum of 32.0 m s^{-1}).

In both model analyses of 10-m winds, the location of the center of the southern cyclone differed from that in the QuikSCAT observations (especially in the NCEP model), but some difference is expected because of translation of the storm center over the approximate 4-h time interval between the 0752 UTC QuikSCAT observations and the 1200 UTC analysis time. It is significant, however, that the two models disagreed on the location of the cyclone center by more than 200 km.

The impact of QuikSCAT data on the OPC manual forecast is shown in Fig. 4. The 0600 UTC surface analysis in the left panel was finalized and transmitted to ships at sea prior to the 0752 UTC overpass of QuikSCAT. Based on earlier QuikSCAT observations, ship observations, and short-term model forecasts (including the NCEP global forecast model), the warning categories in the 0600 UTC forecast were underestimated as gale force for both of the cyclones. The limited number of ship observations available in the area of the two cyclones is typical of this region for this time of year. Based solely on the availability of data from the 0752 UTC QuikSCAT overpass, the forecaster preparing the 1200 UTC manual surface analysis (right panel of Fig. 4) upgraded the wind warning for the southern cyclone by two categories from gale force to hurricane force and upgraded the wind warning for the northern cyclone from gale force to storm force. Without QuikSCAT data, the severity of these cyclones would not have been known to the OPC forecasters and it would not have been possible to issue adequate wind warnings to mariners.

It is noteworthy that the minimum sea level pressure (SLP) in the area of the southern cyclone did not change significantly between the 0600 and 1200 UTC manual OPC analyses; the central pressure was 997 hPa in the 0600 UTC analysis and 996 hPa in the 1200 UTC analysis. Thus, while the QuikSCAT data dramatically altered the wind analysis, they had little impact on the SLP analysis. This is a common occurrence in the manual OPC analyses, which suggests hesitancy on the part of the analyst to depart significantly from the central pressures indicated from the numerical model analyses and the short-term forecasts of the NCEP global model.

In an effort to utilize the QuikSCAT data more effectively in the SLP analyses, the OPC recently began using the University of Washington (UW) planetary boundary layer (PBL) model (Patoux and Brown 2003) to estimate SLP from QuikSCAT data. These QuikSCAT-based SLP estimates are used as a first guess for the OPC manual analyses. When run for this particular case study, the UW PBL model estimated the central pressure of the southern cyclone as 988 hPa, which is 10

rowave satellite measurements of SST from the Tropical Rainfall Measuring Mission (TRMM) Microwave Imager (Wentz et al. 2000) and the Advanced Microwave Scanning Radiometer on the NASA Earth Observing System (EOS) *Aqua* satellite (AMSR-E; Chelton and Wentz 2005) have revealed that a strong SST influence on surface winds occurs in regions of strong SST gradients throughout the World Ocean [see the reviews by Xie (2004) and Chelton et al. (2004), and the recent application of AMSR-E data in the south Indian Ocean by O'Neill et al. (2005)]. Although the air-sea interaction processes that are responsible for the observed correlation between SST and low-level winds are not completely understood, it is believed that SST influence on boundary layer stability and vertical mixing plays a preeminent role. Sweet et al. (1981), Jury and Walker (1988), and Wallace et al. (1989) have hypothesized that enhanced vertical turbulent mixing over warm water mixes momentum downward from aloft to the sea surface, accelerating the surface winds. Conversely, stabilization of the boundary layer over cold water reduces turbulent mixing, thus decoupling the surface winds from the winds aloft and decelerating the surface winds. Samelson et al. (2006) point out deficiencies in this "momentum mixing hypothesis" for the case of cold deceleration and suggest an alternative, quasi-equilibrium model that offers a possible explanation for both the warm acceleration and the cold deceleration. Small et al. (2005) suggest that secondary circulations driven by SST-induced pressure gradients may also play a role.

The atmospheric boundary layer processes responsible for the observed influence of SST on surface winds are thus the subject of ongoing research. Regardless of the detailed dynamics and thermodynamics of the SST influence on the atmospheric boundary layer, the observed coupling between SST and surface winds in the vicinity of meandering SST fronts is underrepresented in global and regional NWP models (Chelton 2005; Chelton et al. 2006; see also Fig. 6 below).

The SST front in the Gulf Stream region is among the strongest found anywhere in the World Ocean. SST-induced spatial variations of the wind field are therefore particularly intense in this region. The wind speed difference across the north wall of the Gulf Stream is often 7 m s^{-1} or more. These abrupt changes in the wind speed can be dangerous to mariners, especially those operating small fishing or sailing vessels. As a typical example of SST influence on surface winds in the Gulf Stream region, we consider a case study that occurred on 16–17 February 2005 when a cold front was moving off the mid-Atlantic coast. The winds were

southwesterly over the waters east and northeast of Cape Hatteras at about 35.5°N , 76°W . On the time and space scales of synoptic weather variability, small-scale structure in the wind field is affected by numerous factors besides SST. During 16–17 February 2005, however, the surface wind field in the vicinity of the Gulf Stream was predominantly influenced by the SST field. For present purposes, the North Wall of the Gulf Stream is defined to be the 17.5°C SST isotherm, as this is a good representation of the location of strongest SST gradient over most of the region of interest in this study.

The 17.5°C SST isotherm as measured by the AMSR-E is shown for 17 February 2005 by the solid black line in all panels of Fig. 6. During the overpass at 2345 UTC on 16 February 2005, QuikSCAT measured winds of $10\text{--}14 \text{ m s}^{-1}$ on the south side of the north wall of the Gulf Stream with a large area of winds in excess of 12.5 m s^{-1} centered near 37°N , 71°W (upper left panel of Fig. 6). On the north side of the north wall, there was a band of low wind speeds in the $4\text{--}7 \text{ m s}^{-1}$ range. The $>7 \text{ m s}^{-1}$ transition from high to low winds occurred over a distance of about 50 km in the QuikSCAT wind field. In reality, this transition likely occurred over a smaller distance (see Fig. 5), but this cannot be determined with the 25-km resolution limitation of the QuikSCAT winds analyzed here.

The 17 February 2005 analysis of 10-m winds for 0000 UTC from the NCEP global forecast model is shown in the upper right panel of Fig. 6. As in the case study considered in section 3a, the excessively smooth character of the NCEP wind field is again readily apparent, despite assimilation of QuikSCAT winds in the model. In addition to the resolution limitations that are inherent to the NCEP model as documented by the wavenumber spectra in Fig. 1, it has been shown by Chelton and Wentz (2005) that the smoothness of the NCEP wind field in the Gulf Stream region is exacerbated by the low resolution of the Reynolds SST fields (Reynolds and Smith 1994; Reynolds et al. 2002) that are used as the ocean surface boundary condition in the NCEP model. SST gradients in the vicinity of the Gulf Stream are underestimated by more than a factor of 2 in the Reynolds analyses (see Figs. 5 and 8 of Chelton and Wentz 2005). The dashed line in the upper right panel of Fig. 6 is the 17.5°C isotherm from the Reynolds SST field. Note that this line separates the region of higher model winds to the south from the band of light model winds to the north, evidence that SST does, in fact, influence the boundary layer winds in the NCEP model. Note also the smoothness of this line compared with the 17.5°C isotherm from the AMSR-E data

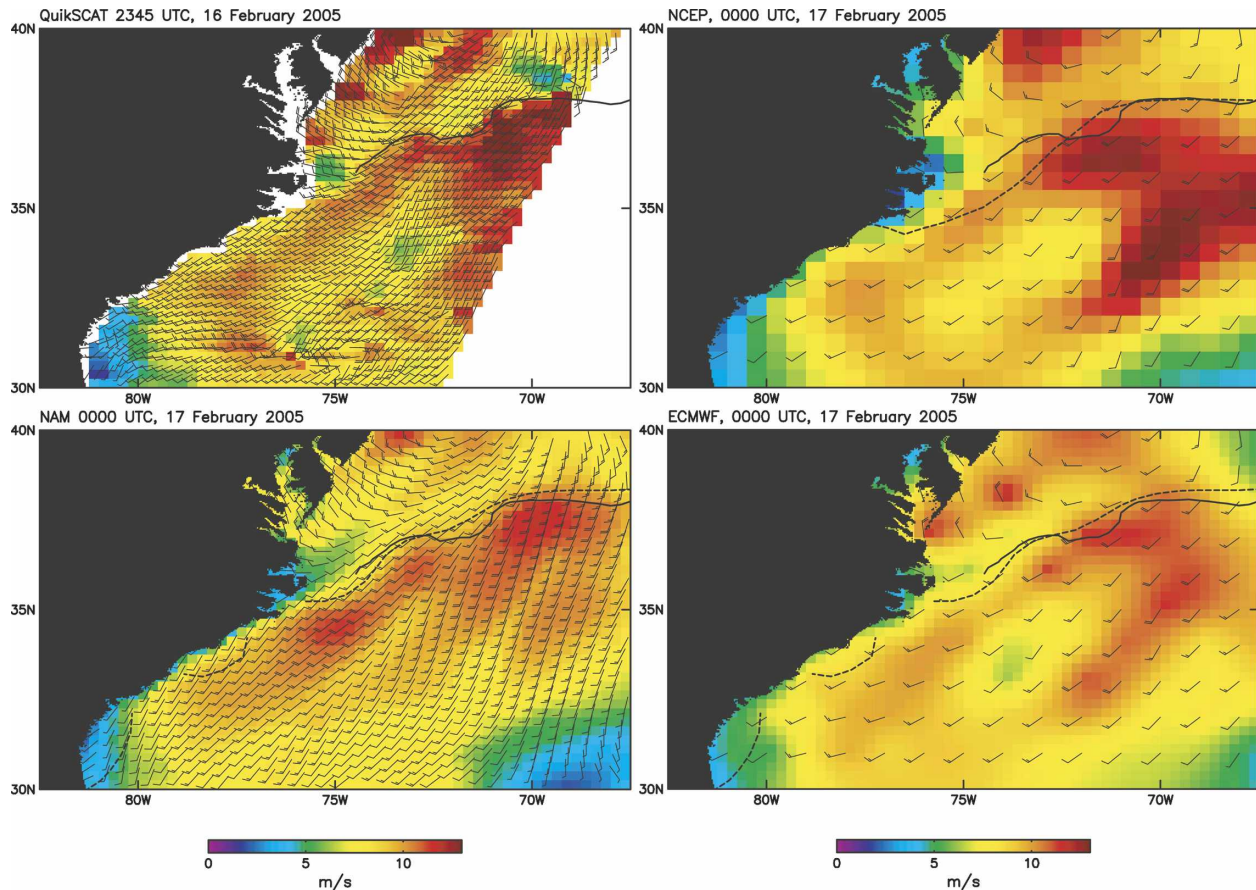


FIG. 6. The wind fields in the western North Atlantic on 17 Feb 2005 constructed for the times indicated on each panel from (upper left) QuikSCAT observations of 10-m winds; (lower left) the 10-m wind analysis by the high-resolution NOAA/NCEP NAM model; (upper right) the 10-m wind analysis by the NCEP global forecast model; and (lower right) the 10-m wind analysis by the ECMWF global forecast model. QuikSCAT wind barbs are plotted on a $0.25^\circ \times 0.25^\circ$ grid, the 12-km NAM wind barbs are plotted on a $36 \text{ km} \times 36 \text{ km}$ grid, and the NCEP and ECMWF wind barbs are plotted on $1^\circ \times 1^\circ$ grids. As in Fig. 3, the wind barbs are in knots and the color scale corresponds to the wind speed in m s^{-1} . Solid black lines in all four panels represent the 17.5°C isotherm as measured by the AMSR-E. Dashed lines represent the 17.5°C isotherms from (upper right) the Reynolds SST analysis and (both bottom panels) the RTG_SST analysis.

shown by the solid line. Because of the underestimates of SST gradients in the Reynolds SST analyses, the transition from higher to lower winds across the 17.5°C isotherm in the NCEP wind field at about 38°N , 70°W is merely 3 m s^{-1} , which is about $1/3$ as large as the change in wind speed measured by QuikSCAT at this location.

The accuracy of the representation of the observed influence of SST on low-level winds in NWP models is very sensitive to specification of the SST boundary condition (Chelton 2005; Chelton and Wentz 2005). This can be inferred from comparison of the right two panels of Fig. 6. The lower right panel is the 0000 UTC analysis of 10-m winds for 17 February 2005 from the ECMWF model. On 9 May 2001, the ocean surface boundary condition in the ECMWF model was changed from the

Reynolds SST analyses to the higher-resolution NOAA real-time global SST analyses (RTG_SST; Thiébaux et al. 2003). The dashed line in the lower right panel of Fig. 6 is the 17.5°C isotherm in the RTG_SST field. While smoother than the true SST fields as measured by AMSR-E, the SST gradients in the RTG_SST fields are a significant improvement over the Reynolds SST fields (Chelton and Wentz 2005). As a result, the ECMWF wind field in the lower right panel of Fig. 6 is somewhat less smooth than the NCEP wind field in the upper right panel (see also Figs. 13–15 of Chelton and Wentz 2005). However, because of its inherently low resolution (Fig. 1), the ECMWF wind field is still considerably smoother than the wind field measured by QuikSCAT, despite assimilation of QuikSCAT winds into the model. The ECMWF model underestimates

the wind response to SST by about a factor of 2 on both sides of the Gulf Stream.

The influence of SST on low-level winds is better represented in higher-resolution NWP models. This is illustrated in the lower left panel of Fig. 6 from the 0000 UTC analysis of 10-m winds on 17 February 2005 from the NOAA/NCEP North American Mesoscale model (NAM, formerly Eta; Rogers et al. 2005), which has a grid resolution of 12 km. QuikSCAT winds are not assimilated into the NAM model. The ocean surface boundary condition in the NAM model was changed from the Reynolds SST analyses to the RTG_SST analyses on 30 January 2001 after tests determined that the higher-resolution SST improved wintertime weather forecasts along the eastern seaboard of the United States (Thiébaux et al. 2003; E. Rogers 2005, personal communication). With the combination of higher-resolution SST and higher model grid resolution, the surface wind field analysis in the NAM model has significantly higher resolution than in the NCEP and ECMWF global forecast models shown in the right panels of Fig. 6. The transition from higher to lower winds occurred over a smaller cross-frontal distance than in the NCEP or ECMWF models. Compared with the QuikSCAT winds in the upper left panel, however, the NAM model still considerably underestimated the high winds on the south side of the Gulf Stream and overestimated the low winds on the north side, especially in the region of strongest SST gradient near 37°N, 71°W in the AMSR-E SST field discussed previously. As a result, the change in wind speed across the north wall of the Gulf Stream was only about half that observed by QuikSCAT.

The factor-of-2 difference between the wind speed changes across the Gulf Stream in the QuikSCAT wind field and in the NAM 10-m wind analysis in the lower left panel of Fig. 6 significantly limits the ability of the NAM model to accurately forecast winds and respondent seas in the vicinity of the Gulf Stream. Because of the availability of QuikSCAT data, OPC forecasters routinely anticipate such conditions in their manual analyses of surface winds in the western North Atlantic, thus producing forecasts that are more accurate than those obtained numerically from the NAM model or from the coarser-resolution NCEP and ECMWF global forecast models.

c. Some comments on the use of QuikSCAT data at the NOAA forecast centers

The successful use of QuikSCAT data in daily forecast operations at the OPC and other NOAA forecast centers is attributable to several factors. Most important are the availability of the QuikSCAT data in near-

real time (NRT)² (within 3 h of the QuikSCAT observations), the accuracy of the measurements, and the wide 1600-km swath with no nadir gap near the satellite ground track. The wide QuikSCAT swath provides more complete coverage of storm systems, which were often only partially sampled in the narrow swath of the scatterometers on the European Remote Sensing *ERS-1* and *ERS-2* satellites and in the dual-swath measurements by NSCAT. The broad QuikSCAT coverage is especially helpful at latitudes higher than about 40° where neighboring measurement swaths overlap (Schlax et al. 2001).

The 25-km NRT QuikSCAT data first became available to OPC forecasters via the Internet in the fall of 1999. Prior to this, it was not possible from the sparsely distributed ship observations to differentiate consistently between high winds (storm force) and extreme winds (hurricane force). OPC forecasters therefore issued only gale-force (17.2–24.4 m s⁻¹) and storm-force (24.5 m s⁻¹ and higher) warnings in their manual surface analyses and text warning bulletins of extratropical storm systems. In December 2000, the OPC expanded the number of extratropical wind warning categories by subdividing the storm-force category into storm force (24.5–32.6 m s⁻¹) and hurricane force (32.7 m s⁻¹ and higher) (Sienkiewicz et al. 2004).

In October 2001, the 25-km NRT QuikSCAT winds became available in the NOAA/NCEP Advanced Weather Interactive Processing System (N-AWIPS) that is used at the OPC and the NOAA/Tropical Prediction Center (TPC). The NRT QuikSCAT winds became available in N-AWIPS at a higher resolution of 12.5 km in December 2003. Between October 2001 and May 2005, OPC forecasters issued warnings for a total of 175 hurricane-force extratropical cyclones in the North Atlantic and North Pacific combined; an example is shown in Fig. 7. Moreover, Von Ahn and Sienkiewicz (2005) found that the availability of QuikSCAT data in 2002–04 resulted in significant increases in the numbers of OPC extratropical wind warnings in each category (especially in the hurricane-force category) compared with what the wind forecasts would have been if QuikSCAT data had not been available to the OPC forecaster (Fig. 8).

² The processing of the NRT QuikSCAT dataset is summarized in section 2b of CF05. The NRT winds differ somewhat from the so-called standard product QuikSCAT winds that are archived for research applications. For the purposes of the discussion here, the differences between the standard product winds shown in Figs. 3 and 6 and the NRT winds assimilated into the NCEP and ECMWF models and used by the forecasters at the OPC are not significant.

MARINE WEATHER DISCUSSION...UPDATE
 NATIONAL WEATHER SERVICE WASHINGTON DC
 OCEAN PREDICTION CENTER/OCEAN FORECAST BRANCH
 631 AM EST MON 27 DEC 2004

.FORECAST DISCUSSION: MAJOR FEATURES/WINDS/SEAS/SIGNIFICANT WEATHER FOR NORTH
 ATLANTIC OCEAN W OF 50W FROM 30N TO 50N

ISSUING QUICK AMEND NEW ENG WATERS FOR SE PTN GLF ME AND GEO BANK ...ISSUING HRCN
 FORCE WRNG.

**LATEST QUIKSCAT DATA SHOWS WINDS TO HRCN FORCE IN SE PTN OF GULF ME AND GEO BANK.
 WILL UPGRADE WINDS TO 50-65 KT SEAS 30-40 FT IN THOSE WATERS.**

WARNINGS...

.NT1 NEW ENGLAND WATERS...UPDATE

.GULF OF MAINE...HRCN FORCE.

.GEORGES BANK...HRCN FORCE.

.S OF NEW ENGLAND...E PTN...STORM E PORTION THIS MRNG...GALE ENDING LATER TODAY.

.W PTN...GALE THIS MORNING ENDING LATER TODAY.

.NT2 MID ATLC WATERS...

.HUDSON TO BALT CYN...STORM...THEN GALE FM W TO E LATER TODAY AND TONIGHT...EXCEPT
 END W PTN.

.BALT TO HATTERAS CYN...STORM EARLY DCRG TO GALE THIS EVENING THEN END TNGT

.HATTERAS CYN TO CAPE FEAR...STORM THIS MORNING DCRG TO GALE LATE TODAY AND ENDING
 BY EVENING.

.CAPE FEAR TO 31N...GALE ENDING THIS MRNG

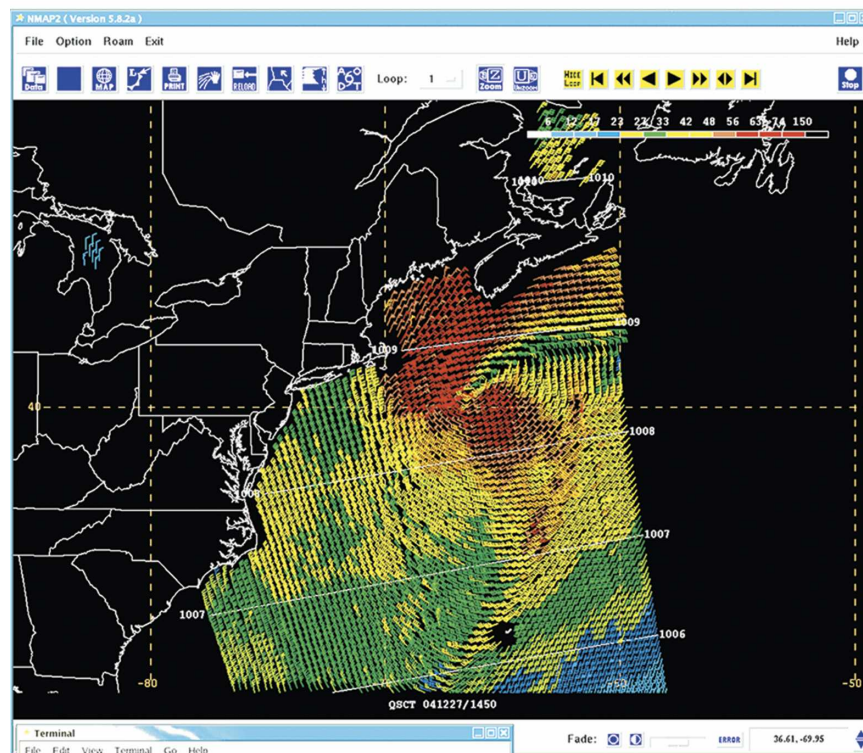


FIG. 7. (top) An example of an extratropical storm warning update bulletin for the western North Atlantic issued on 27 Dec 2004 by the OPC that explicitly references QuikSCAT (highlighted in red for present purposes). (bottom) A screen dump of the N-AWIPS computer display of wind vectors from the QuikSCAT overpass display that was the basis for the update bulletin. The red area corresponds to hurricane-force winds.

The higher-resolution 12.5-km NRT QuikSCAT winds have proven to be significantly more useful than the 25-km winds for forecasts issued by the OPC and TPC. They allow improved definition of the wind field in hurricanes and in the vicinity of orographically influ-

enced flows such as those through straits and passages, near capes, and offshore of mountain gaps (such as the winds that blow westward through the mountain passes in Central America and out over the eastern Pacific). The 12.5-km retrievals also accentuate the wind speed

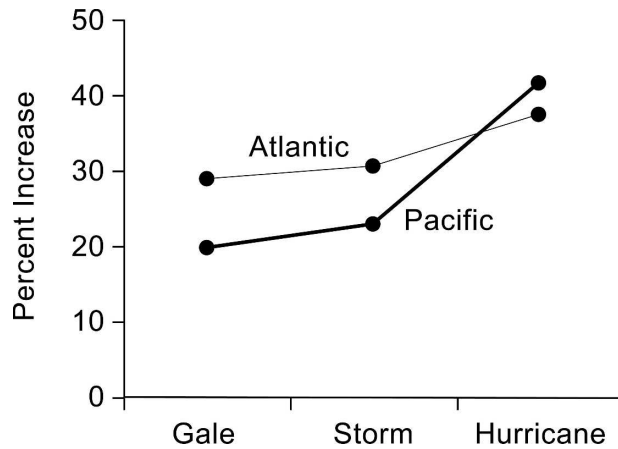


FIG. 8. The percentage increases in the numbers of OPC extra-tropical wind warnings by category for the Atlantic (thin line) and Pacific (heavy line) during 2002 compared with what the wind forecasts would have been if QuikSCAT data had not been available to the OPC forecasters.

differences across strong SST fronts such as the Gulf Stream considered in section 3b.

Knabb (2005) has summarized the use of 12.5-km NRT QuikSCAT data at the TPC during the 2004 hurricane season. These QuikSCAT winds were examined by TPC forecasters in nearly 75% of all forecast cycles, resulting in analysts' decisions to increase predicted wind speeds in approximately 65% of the cases. QuikSCAT measurements were explicitly mentioned in 47 official Tropical Cyclone Discussion (TCD) products issued by the National Hurricane Center for the Atlantic basin and in 43 TCD products for the eastern Pacific sector. Although statistics on the use of QuikSCAT data have not yet been compiled for the 2005 hurricane season, QuikSCAT was frequently cited in the TPC forecast advisories (see <http://www.nhc.noaa.gov/archive/2005/index.shtml>). An example of the use of QuikSCAT data for Hurricane Katrina is shown in Fig. 9.

In spring 2004, 25-km NRT QuikSCAT data were integrated into operational build 4 of the general AWIPS system that is used by the NOAA Weather Forecast Offices (WFOs) throughout the United States. Through AWIPS, forecasters are able to view QuikSCAT winds along with numerical model output, observations, and satellite cloud and SST imagery, all on the same computer screen. For coastal and marine forecasts, the 25-km QuikSCAT winds are often used as an underlay to aid in accurately placing a front on a surface analysis. As the WFO forecasters continue to gain more familiarity with the QuikSCAT data, it is anticipated that these data will become ever more important in the daily decision-making process at the coastal and

nearshore WFOs. The higher-resolution 12.5-km NRT QuikSCAT data may be integrated into a future Operational Build of the AWIPS system.

4. Rain considerations

Scatterometer measurements of radar backscatter can be contaminated by rain effects when there is significant precipitation within the antenna field of view. The QuikSCAT measurements of radar return can be corrupted by scattering and absorption by raindrops in the atmosphere, as well as by increases in radar backscatter from centimetric roughness on the sea surface caused by raindrops hitting the ocean surface (CF05). Tournadre and Quilfen (2003) have shown that the atmospheric effects of raindrops are more significant at the Ku-band frequencies of the NSCAT and QuikSCAT scatterometers than at the C-band frequencies of the *ERS-1* and *ERS-2* scatterometers and the Advanced Scatterometer (ASCAT) to be launched on the European Meteorological Operational (MetOp) satellites beginning in June 2006. As the atmospheric and surface effects of raindrops are not necessarily correlated with wind conditions, the accuracy of wind retrievals calculated from QuikSCAT measurements under raining conditions can be degraded (see Fig. 5 of CF05). A rain flag is therefore reported for each QuikSCAT wind measurement in the NRT and standard product datasets based on the multidimensional histogram-based "MUDH" algorithm described by Huddleston and Stiles (2000) and Stiles and Yueh (2002).

Localized rain is often associated with intense cyclonic systems (Milliff et al. 2004). Many of the QuikSCAT measurements shown in Fig. 1b of Leslie and Buckley (2006) have the rain flag set. Despite the likely presence of rain, these flagged retrievals appear to be realistic estimates of vector winds. Likewise, there were rain-flagged measurements in the case study considered here in section 3a that appear to be realistic wind retrievals. It is therefore of interest to characterize the accuracy of rain-flagged QuikSCAT data in order to assess their utility for operational forecasting.

The ongoing 6.5-yr duration of the QuikSCAT mission and the wide QuikSCAT measurement swath have provided many collocations with open-ocean meteorological buoys. While the accuracies reported in CF05 were based on only the rain-free collocations, there were also a significant number of collocations for which the QuikSCAT rain flag was set. For true (buoy) wind speeds higher than about 13 m s^{-1} , it can be seen from the wind speed and direction comparisons in Fig. 10 that the rain-flagged QuikSCAT accuracy is negligibly worse than for rain-free measurements (see also Milliff

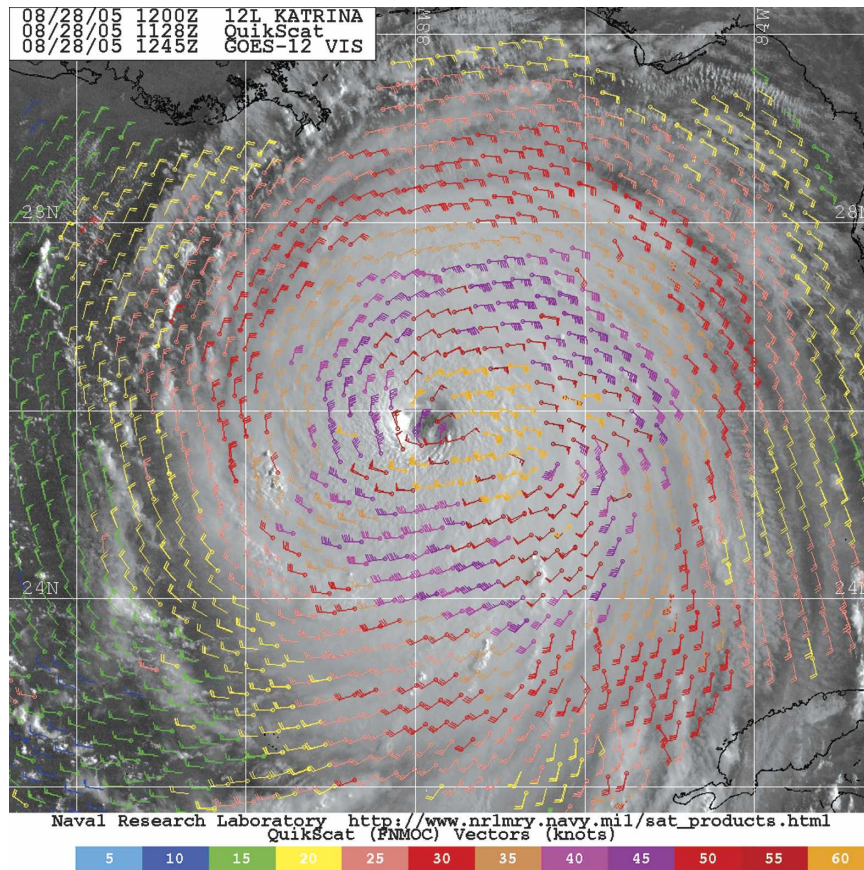


FIG. 9. An example of QuikSCAT observations of 10-m winds used operationally at the TPC. This overlay of NRT 12.5-km QuikSCAT wind estimates on visible cloud imagery from a geostationary satellite for Hurricane Katrina near its peak intensity on 28 Aug 2005 was produced by the Naval Research Laboratory in Monterey, CA. Although heavy rains degrade the accuracy of the scatterometer data, the measurements in high-wind conditions outside the intense hurricane core contain quantitatively useful information as discussed in section 4. (Courtesy of J. Beven, NOAA TPC.)

et al. 2004). For lower true wind speeds, however, the presence of rain decreases the scatterometer sensitivity to wind speed and increasingly biases the QuikSCAT speed estimates high with decreasing wind speed (top panel of Fig. 10). Moreover, the scatterometer directional accuracy is substantially degraded under raining conditions when the true wind speed is less than about 13 m s^{-1} (lower panel of Fig. 10).

The multiyear QuikSCAT–buoy comparisons thus suggest that rain-flagged QuikSCAT wind speed and direction estimates are often accurate if it is known a priori that the true wind speed exceeds about 13 m s^{-1} , and this indeed appears to be the case in the example shown in Fig. 3 of this study and in Fig. 1b of Leslie and Buckley (2006). The backscatter from the wind-roughened sea surface can evidently override the contaminating effects of rain in high-wind conditions, thus resulting in accurate wind retrievals. In lower wind con-

ditions, however, raindrops in the atmosphere and rain-induced roughness of the sea surface dominate the backscatter measured by QuikSCAT, resulting in erroneously high wind speed estimates (top panel of Fig. 10).

Users are cautioned that QuikSCAT wind estimates alone cannot be used to ascertain whether a rain-flagged observation is a valid estimate of the wind since high winds can be either valid or erroneous, depending on the true wind speed. To assess whether the true wind speed is high or low, additional information is required, either from in situ measurements as in the buoy comparisons in Fig. 10, or based on the judgment of an experienced analyst.

The problem of identifying which flagged QuikSCAT observations are legitimate becomes clear from Fig. 11. At any given true (buoy) wind speed higher than about 13 m s^{-1} , the distribution of QuikSCAT wind speeds (i.e., a vertical slice through Fig. 11) is approximately

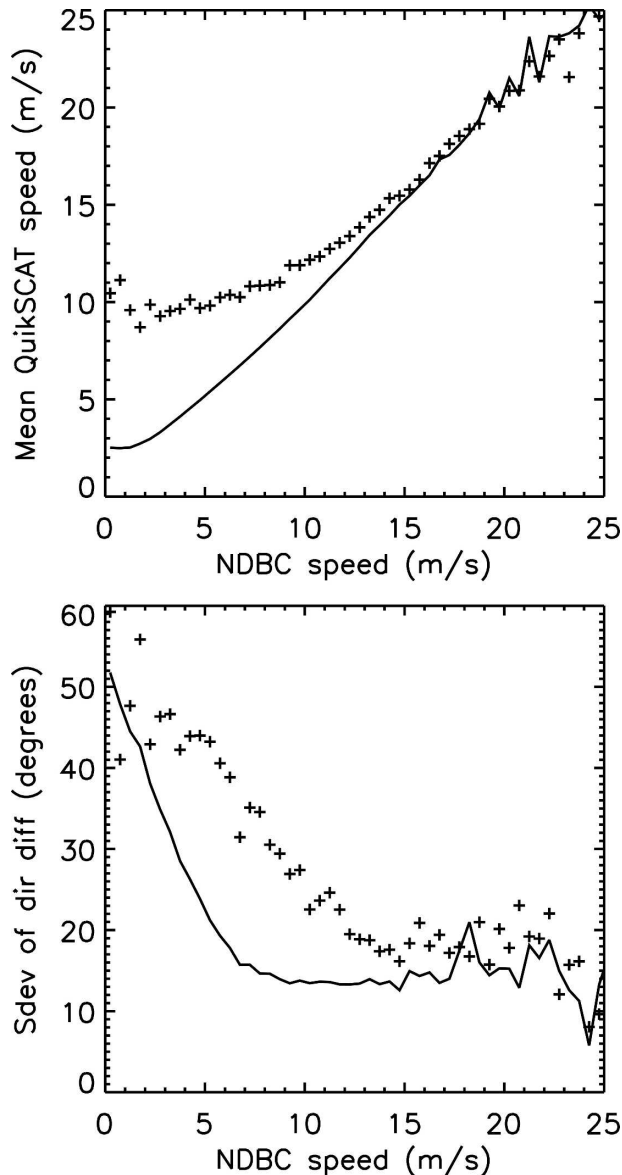


FIG. 10. QuikSCAT wind speeds and directions compared with collocated buoy measurements: (top) conditional mean scatterometer speeds binned on buoy speed and (bottom) standard deviations of buoy minus scatterometer wind direction differences as a function of buoy wind speed. The plus symbols correspond to rain-flagged QuikSCAT observations, and the lines represent rain-free QuikSCAT observations. The noisiness at high wind speeds is likely attributable to statistical uncertainties owing to the much smaller number of collocations. The QuikSCAT winds are reported as equivalent neutral-stability winds at 10 m. For these comparisons, the buoy winds were converted to equivalent neutral stability winds at 10 m as described in CF05.

symmetric and narrowly peaked around the true wind speed. At lower true wind speeds, the distribution of QuikSCAT estimates are skewed toward higher wind speeds. In low-wind conditions, there are thus many

rain-flagged QuikSCAT wind speed estimates in excess of 13 m s^{-1} that are erroneously high.

Distinguishing valid wind estimates from rain-contaminated estimates requires careful analysis by a trained analyst. The fact that rain-contaminated data tend to have directions oriented across track (see Fig. 5 of CF05) is often useful in this regard and is one of the attributes considered in the MUDH rain flag algorithm. The buoy comparisons and case studies presented here and in other studies (e.g., Milliff et al. 2004) suggest that the MUDH rain flag can be overly conservative in high-wind conditions. When the presence of rain is likely, QuikSCAT often produces realistic estimates of the surface wind speed and direction if the true wind speed exceeds about 13 m s^{-1} . The use of such flagged but high wind speed data by Leslie and Buckley (2006) and in the case study considered in section 3a of this study thus appear to be justified.

5. Conclusions and outlook for the future

The value of scatterometry for weather forecasting was illustrated from consideration of two extratropical case studies in the Northern Hemisphere. One of these was an intense cyclone in the western North Pacific and the other was a case of moderate winds in the western North Atlantic. In both cases, the 10-m wind analyses from the NCEP and ECMWF global forecast models considerably underestimated the spatial variability on scales smaller than about 1000 km, despite the fact that both models assimilated QuikSCAT measurements of surface winds. The information content of the QuikSCAT data is thus underutilized in the NWP models. Forecasters at the NOAA/NCEP OPC, the TPC, and other NOAA WFOs around the U.S. coast recognize the value of QuikSCAT winds and routinely incorporate QuikSCAT data in their manual surface analyses. Their warning bulletins often make explicit reference to QuikSCAT as the basis for high-wind warnings (e.g., Fig. 7).

As long-time protagonists of scatterometry, it is gratifying to see that scatterometer data are now routinely used by operational weather forecasters and by researchers such as Leslie and Buckley (2006) who are not deeply versed in the technical details of scatterometry. However, after more than 25 yr of sustained effort toward establishing an operational scatterometer system for global weather forecasting and climate research, it is disheartening that the future of high-quality satellite measurements of surface vector winds over the ocean is less encouraging now than it was a decade ago (Kelly 2004).

QuikSCAT was launched in June 1999 with a 3-yr

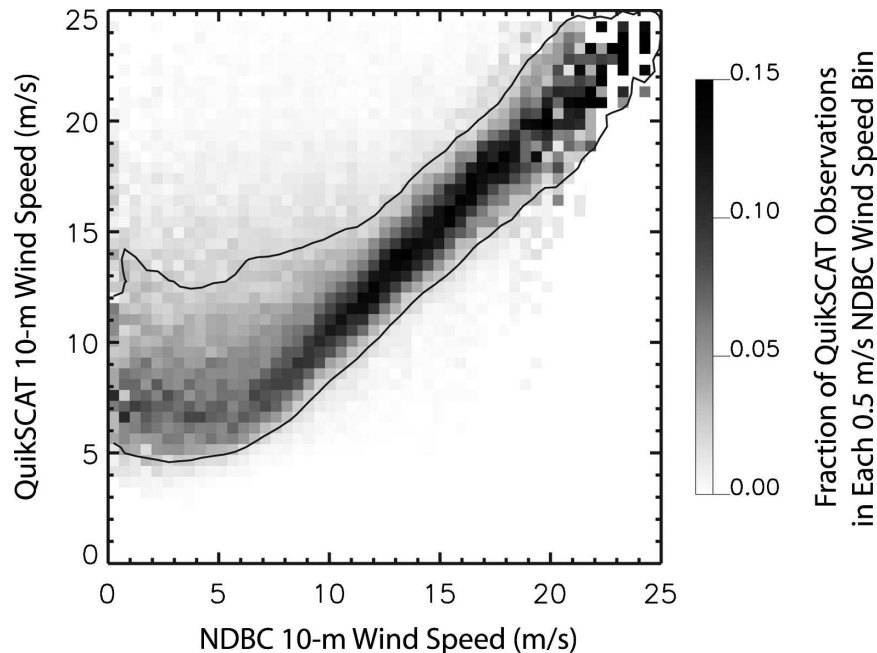


FIG. 11. The distribution of rain-flagged QuikSCAT wind speeds as a function of buoy wind speed. The histogram of QuikSCAT wind speeds within each 0.5 m s^{-1} buoy wind speed bin was normalized to sum to 1. The contour corresponds to normalized histogram values of 0.025. The buoy winds were converted to equivalent neutral stability winds at 10 m as described in CF05. Note that the number of collocations in raining conditions becomes small at wind speeds higher than about 20 m s^{-1} .

mission design and a 5-yr instrument lifetime. The QuikSCAT mission has now lasted 7 yr. In spite of considerable effort to establish a scatterometer mission to succeed QuikSCAT, there are presently no plans in the United States to launch future scatterometers. The European Space Agency will launch a series of C-band ASCAT scatterometers as part of the MetOp operational satellite program that is scheduled to begin in June 2006. While the measurement accuracy of ASCAT is essentially the same as that of the Ku-band SeaWinds scatterometer on QuikSCAT, and ASCAT is less sensitive to rain contamination, the swath coverage is about 1/3 less than that of QuikSCAT (Schlax et al. 2001). Moreover, the ASCAT sampling in the final design consists of two parallel 550-km swaths separated by a wide gap of 720 km. As noted in section 3c, the experience of operational forecasters is that the continuous 1600-km swath of QuikSCAT has been particularly beneficial for prediction of marine weather systems; the 330-km nadir gap of the dual-swath NSCAT scatterometer (the NASA predecessor to QuikSCAT) was problematic for operational applications. The much wider 720-km nadir gap in the ASCAT measurement swath is therefore likely to present even greater challenges for operational forecasting.

Future U.S. satellite measurements of ocean vector winds will be obtained from the National Polar-Orbiting Operational Environmental Satellite System (NPOESS; Glackin et al. 2004). NPOESS was established by a May 1994 presidential directive to converge the existing civilian and military polar-orbiting environmental satellite systems from NOAA [the Polar-orbiting Operational Environmental Satellite program (POES)] and the Air Force [the Defense Meteorological Satellite Program (DMSP)], as well as NASA research satellites. The objective of this merging of satellite programs was to reduce the costs of acquiring and operating these systems while continuing to satisfy U.S. operational satellite data requirements.

As originally envisioned, NPOESS consisted of a series of six satellites, the first of which was to launch in 2009, with subsequent satellite launches at 18–19-month intervals. The launch date for the first NPOESS satellite has slipped several times and is now tentatively scheduled for 2012, but is expected to slip even further (Zielinski 2005). The primary reason for the launch delays and a cost overrun of at least 15% is engineering problems with the Visible/Infrared Imager/Radiometer Suite (VIIRS). There are also problems with several of the other instruments onboard NPOESS (Butler 2005).

The emphasis in NPOESS is on operational needs, with research requirements of secondary concern. The research community thus had little input to the planning for the NPOESS system. The requirements for all of the variables to be measured by the instruments on the NPOESS satellites are specified in the Integrated Operational Requirements Document (IORD) (http://npoesslib.ipo.noaa.gov/IPOarchive/MAN/IORDII_011402.pdf). Most research and operational applications of satellite measurements of ocean winds require both wind speed and direction. In the IORD specification for ocean winds, only wind speed is considered a “Key Performance Parameter” that is critical to the success of the NPOESS mission; failure to meet the wind direction threshold specification in the IORD will not trigger reassessment or reevaluation of the NPOESS system.

Rather than adopting the mature and proven technique of radar scatterometry, NPOESS chose the developmental and unproven technology of passive polarimetric radiometry as the approach for measurements of ocean vector winds (Yueh et al. 1997, 1999; Gaiser et al. 2004). The particular polarimetric radiometer on NPOESS is the Conical Microwave Imager/Sounder (CMIS). CMIS is among the instruments that are contributing to the delays in the launch date for the first NPOESS satellite. There is a possibility that CMIS may be excluded from the initial launch payload in order to accommodate the cost and schedule overruns currently plaguing the overall mission. None of the other instruments in the NPOESS payload are capable of measuring vector winds.

At the time the decision was made to adopt CMIS for operational measurements of ocean vector winds, a polarimetric radiometer had not yet been flown in space. The detailed measurement characteristics of polarimetric estimates of ocean vector winds that are of interest to the operational and research communities are still not known. In preparation for CMIS, the U.S. Navy launched the WindSat polarimetric radiometer in January 2003 as a “risk reduction demonstration project” (Gaiser et al. 2004). Though not identical to CMIS, the WindSat radiometer is similar enough that it is providing useful insight into the performance that can be expected from CMIS.

Efforts are underway to determine the wind speed and directional accuracy of WindSat retrievals over a wide range of environmental conditions. Six months (September 2002–February 2003) of WindSat estimates of vector winds based on an initial wind retrieval algorithm were released to the public in August 2004. Analyses indicate that the errors of these WindSat wind estimates are about 30% larger than the QuikSCAT

measurement errors (Freilich and Vanhoff 2006; Monaldo 2006). While the WindSat measurement accuracy is likely to improve with refinements of the retrieval algorithms, it is not yet known whether it will match the accuracy of scatterometer wind retrievals. Global WindSat estimates of vector winds from all four seasons based on an updated wind retrieval algorithm have only recently (January 2006) been made available for community analysis. It is therefore not yet possible to anticipate the wind speed and direction accuracy that may be obtainable from CMIS if it is included in the launch payload of the first NPOESS satellite.

Acknowledgments. We thank Michael Schlax and Barry Vanhoff for data processing support and for help with the figures. We also thank John Beven, Paul Chang, Hans Hersbach, Steve Lord, and Joe Sela for valuable contributions to this study. This paper benefited from the presentations and discussion at the Satellite Measurements of Ocean Vector Winds Workshop sponsored by the Cooperative Institute for Oceanographic Satellite Studies (<http://cioss.coas.oregonstate.edu/CIOSS/index.html>) and hosted by the NOAA Tropical Prediction Center in Miami, Florida. This research was supported by NASA Grant NAS5-32965 for funding of Ocean Vector Winds Science Team activities, Award NA03NES4400001, to Oregon State University from the National Oceanic and Atmospheric Administration, U.S. Department of Commerce, and by the National Oceanographic Partnership Program funding under Scatterometer-Derived Operational Winds, Surface Pressures, and Rain through the NOAA/National Environmental Satellite, Data, and Information Service (NESDIS). The statements, findings, conclusions, and recommendations are those of the authors and do not necessarily reflect the views of NOAA or the Department of Commerce.

REFERENCES

- Atlas, R., and Coauthors, 2001: The effects of marine winds from scatterometer data on weather analysis and forecasting. *Bull. Amer. Meteor. Soc.*, **82**, 1965–1990.
- , A. Y. Hou, and O. Reale, 2005a: Application of SeaWinds scatterometer and TMI-SSM/I rain rates to hurricane analysis and forecasting. *Photogramm. Remote Sens.*, **59**, 233–243.
- , and Coauthors, 2005b: Hurricane forecasting with the high-resolution NASA finite volume general circulation model. *Geophys. Res. Lett.*, **32**, L03807, doi:10.1029/2004GL021513.
- Butler, A., 2005: Posing a setback. *Aviation Week*, **162**, 68–69.
- Chelton, D. B., 2005: The impact of SST specification on ECMWF surface wind stress fields in the eastern tropical Pacific. *J. Climate*, **18**, 530–550.
- , and M. H. Freilich, 2005: Scatterometer-based assessment of 10-m wind analyses from the operational ECMWF and

- NCEP numerical weather prediction models. *Mon. Wea. Rev.*, **133**, 409–429.
- , and F. J. Wentz, 2005: Global microwave satellite observations of sea-surface temperature for numerical weather prediction and climate research. *Bull. Amer. Meteor. Soc.*, **86**, 1097–1115.
- , M. G. Schlax, M. H. Freilich, and R. F. Milliff, 2004: Satellite measurements reveal persistent small-scale features in ocean winds. *Science*, **303**, 978–983.
- , —, and R. M. Samelson, 2006: Summertime coupling between sea surface temperature and wind stress in the California current system. *J. Phys. Oceanogr.*, in press.
- Cornillon, P., and D. R. Watts, 1987: Satellite thermal infrared and inverted echo sounder determinations of the Gulf Stream northern edge. *J. Atmos. Oceanic Technol.*, **4**, 712–723.
- Freilich, M. H., and D. B. Chelton, 1986: Wavenumber spectra of Pacific winds measured by the Seasat scatterometer. *J. Phys. Oceanogr.*, **16**, 741–757.
- , and R. S. Dunbar, 1999: The accuracy of the NSCAT-1 vector winds: Comparisons with National Data Buoy Center buoys. *J. Geophys. Res.*, **104**, 11 231–11 246.
- , and B. A. Vanhoff, 2006: The accuracy of the preliminary WindSat vector wind measurements: Comparisons with NDBC buoys and QuikSCAT. *IEEE Trans. Geosci. Remote Sens.*, **44**, 622–637.
- Gaiser, P. W., and Coauthors, 2004: The WindSat spaceborne polarimetric microwave radiometer: Sensor description and early orbit performance. *IEEE Trans. Geosci. Remote Sens.*, **42**, 2347–2361.
- Glackin, D. L., J. D. Cunningham, and C. S. Nelson, 2004: Earth remote sensing with NPOESS: Instruments and environmental data products. *Proc. SPIE*, **5234**, 123–131.
- Huddleston, J. N., and B. W. Stiles, 2000: Multidimensional histogram (MUDH) rain flag product description (version 3.0). Jet Propulsion Laboratory, Pasadena, CA, 17 pp. [Available online at ftp://podaac.jpl.nasa.gov/pub/ocean_wind/quikscat/L2B/doc/MUDH_Description_V3.pdf.]
- Isaksen, L., and P. A. E. M. Janssen, 2004: Impact of ERS scatterometer winds in ECMWF's assimilation system. *Quart. J. Roy. Meteor. Soc.*, **130**, 1793–1814.
- Jury, M. R., and N. Walker, 1988: Marine boundary layer modification across the edge of the Agulhas Current. *J. Geophys. Res.*, **93**, 647–654.
- Kelly, K. A., 2004: Wind data: A promise in peril. *Science*, **303**, 962–963.
- Knabb, R., cited 2005: Impacts of QuikSCAT on Tropical Prediction Center operations. [Available online at http://cioss.coas.oregonstate.edu/CIOSS/workshops/miami_meeting/Miami_Presentations/17_Knabb_TPC_impacts_of_qscat.ppt.]
- Leidner, S. M., L. Isaksen, and R. N. Hoffman, 2003: Impact of NSCAT winds on tropical cyclones in the ECMWF 4DVAR assimilation system. *Mon. Wea. Rev.*, **131**, 3–26.
- Leslie, L. M., and B. W. Buckley, 2006: Comments on “Scatterometer-based assessment of 10-m wind analyses from the operational ECMWF and NCEP numerical weather prediction models.” *Mon. Wea. Rev.*, **134**, 737–742.
- Milliff, R. F., W. G. Large, J. Morzel, G. Danabasoglu, and T. M. Chin, 1999: Ocean general circulation model sensitivity to forcing from scatterometer winds. *J. Geophys. Res.*, **104C**, 11 337–11 358.
- , J. Morzel, D. B. Chelton, and M. H. Freilich, 2004: Wind stress curl and wind stress divergence biases from rain effects on QSCAT surface wind retrievals. *J. Atmos. Oceanic Technol.*, **21**, 1216–1231.
- Monaldo, F. M., 2006: Evaluation of WindSat wind vector performance with respect to QuikSCAT estimates. *IEEE Trans. Geosci. Remote Sens.*, **44**, 638–644.
- O'Neill, L. W., D. B. Chelton, S. K. Esbensen, and F. J. Wentz, 2005: High-resolution satellite observations of SST modification of the marine atmospheric boundary layer over the Agulhas Return Current. *J. Climate*, **18**, 2706–2723.
- Patoux, J., and R. A. Brown, 2001: Spectral analysis of QuikSCAT surface winds and two-dimensional turbulence. *J. Geophys. Res.*, **106D**, 23 995–24 005.
- , and —, 2003: Global pressures from scatterometer winds. *J. Appl. Meteor.*, **42**, 813–826.
- Portabella, M., and A. Stoffelen, 2004: A probabilistic approach for SeaWinds data assimilation. *Quart. J. Roy. Meteor. Soc.*, **130**, 127–152.
- Reynolds, R. W., and T. M. Smith, 1994: Improved global sea surface temperature analyses using optimum interpolation. *J. Climate*, **7**, 929–948.
- , N. A. Rayner, T. M. Smith, D. C. Stokes, and W. Wang, 2002: An improved in situ and satellite SST analysis for climate. *J. Climate*, **15**, 1609–1625.
- Rogers, E., and Coauthors, 2005: The NCEP North American Mesoscale Modeling System: Final Eta Model/analysis changes and preliminary experiments using the WRF-NMM. Preprints, *21st Conf. on Weather Analysis and Forecasting/17th Conf. on Numerical Weather Prediction*, Washington, DC, Amer. Meteor. Soc., CD-ROM, 4B.5.
- Samelson, R. M., E. D. Skyllingstad, D. B. Chelton, S. K. Esbensen, L. W. O'Neill, and N. Thum, 2006: On the coupling of wind stress and sea surface temperature. *J. Climate*, **19**, 1557–1566.
- Schlax, M. G., D. B. Chelton, and M. H. Freilich, 2001: Sampling errors in wind fields constructed from single and tandem scatterometer datasets. *J. Atmos. Oceanic Technol.*, **18**, 1014–1036.
- Sharp, R. J., M. A. Bourassa, and J. J. O'Brien, 2002: Early detection of tropical cyclones using SeaWinds-derived vorticity. *Bull. Amer. Meteor. Soc.*, **83**, 879–889.
- Sienkiewicz, J. M., J. M. Von Ahn, and G. M. McFadden, 2004: Hurricane force extratropical cyclones. Preprints, *21st Conf. on Weather Analysis and Forecasting/17th Conf. on Numerical Weather Prediction*, Seattle, WA, Amer. Meteor. Soc., CD-ROM, 4A.3.
- Small, R. J., S.-P. Xie, Y. Wang, S. K. Esbensen, and D. Vickers, 2005: Numerical simulation of boundary layer structure and cross-equatorial flow in the eastern Pacific. *J. Atmos. Sci.*, **62**, 1812–1830.
- Stiles, B. W., and S. H. Yueh, 2002: Impact of rain on spaceborne Ku-band wind scatterometer data. *IEEE Trans. Geosci. Remote Sens.*, **40**, 1973–1983.
- Sweet, W. R., R. Fett, J. Kerling, and P. La Violette, 1981: Air–sea interaction effects in the lower troposphere across the north wall of the Gulf Stream. *Mon. Wea. Rev.*, **109**, 1042–1052.
- Thiébaux, J., E. Rogers, W. Wang, and B. Katz, 2003: A new high-resolution blended real-time global sea surface temperature analysis. *Bull. Amer. Meteor. Soc.*, **84**, 645–656.
- Tournadre, J., and Y. Quilfen, 2003: Impact of rain cell on scatterometer data: 1. Theory and modeling. *J. Geophys. Res.*, **108**, 3225, doi:10.1029/2002JC001428.
- Von Ahn, J. M., and J. M. Sienkiewicz, 2005: The operational

- impact of QuikSCAT winds at the National Oceanic and Atmospheric Administration Ocean Prediction Center. *Proc. IGARSS'04*, Vol. 5, Anchorage, AK, IEEE, 3180–3183.
- Wallace, J. M., T. P. Mitchell, and C. Deser, 1989: The influence of sea surface temperature on surface wind in the eastern equatorial Pacific: Seasonal and interannual variability. *J. Climate*, **2**, 1492–1499.
- Wentz, F. J., C. Gentemann, D. Smith, and D. Chelton, 2000: Satellite measurements of sea surface temperature through clouds. *Science*, **288**, 847–850.
- Wikle, C. K., R. F. Milliff, and W. G. Large, 1999: Surface wind variability on spatial scales from 1 to 1000 km observed during TOGA COARE. *J. Atmos. Sci.*, **56**, 2222–2231.
- Xie, S.-P., 2004: Satellite observations of cool ocean–atmosphere interaction. *Bull. Amer. Meteor. Soc.*, **85**, 195–208.
- Yeh, H.-C., T.-J. George, and W. T. Liu, 2002: Kinematic characteristics of a mei-yu front detected by the QuikSCAT oceanic winds. *Mon. Wea. Rev.*, **130**, 700–711.
- Yueh, S. H., W. J. Wilson, F. K. Li, W. B. Ricketts, and S. V. Nghiem, 1997: Polarimetric brightness temperatures of sea surfaces measured with aircraft K- and Ka-band radars. *IEEE Trans. Geosci. Remote Sens.*, **33**, 1177–1187.
- , —, S. J. DiNardo, and F. K. Li, 1999: Polarimetric brightness signatures of ocean wind direction. *IEEE Trans. Geosci. Remote Sens.*, **37**, 949–959.
- Zielinski, S., 2005: Environmental satellite program over budget, behind schedule. *Eos, Trans. Amer. Geophys. Union*, **86**, 446.